Amino Acids (2011) 41:733–742
DOI 10.1007/s00726-011-0941-z

ORIGINAL ARTICLE

A systematic study of fundamentals in α-helical coiled coil mimicry by alternating sequences of β- and γ-amino acids

Raheleh Rezaei Araghi · Carsten Baldauf · Ulla I. M. Gerling · Cosimo Damiano Cadicamo · Beate Koksch

Received: 25 February 2011 / Accepted: 11 May 2011 / Published online: 3 June 2011

Abstract Aimed at understanding the crucially important structural features for the integrity of α-helical mimicry by βγ-sequences, an α-amino acid sequence in a native peptide was substituted by differently arranged βγ-sequences. The self- and hetero-assembly of a series of αβγ-chimeric sequences based on a 33-residue GCN4-derived peptide was investigated by means of molecular dynamics, circular dichroism, and a disulfide exchange assay. Despite the native-like behavior of βγ alternating sequences such as retention of α-helix dipole and the formation of 13-membered α-helix turns, the αβγ-chimeras with different βγ substitution patterns do not equally mimic the structural behavior of the native parent peptide in solution. The preservation of the key residue contacts such as van der Waals interactions and intrahelical H-bonding, which can be met only by particular substitution patterns, thermodynamically favor the adoption of coiled coil folding motif. In this study, we show how successfully the destabilizing structural consequences of α → βγ modification can be harnessed by reducing the solvent-exposed hydrophobic surface area and placing of suitably long and bulky helix-forming side chains at the hydrophobic core. The pairing of αβγ-chimeric sequences with the native wild-type are thermodynamically allowed in the case of ideal arrangement of β- and γ-residues. This indicates a similarity in local side chain packing of β- and γ-amino acids at the helical interface of αβγ-chimeras and the native α-peptide. Consequently, the backbone extended residues are able to participate in classical "knob-into-hole" packing with native α-peptide.

Keywords α-Helical coiled coil · Foldamers · Chimeric peptides · β-Amino acids · γ-Amino acids

Abbreviations

CD	Circular dichroism
AU	Analytical ultracentrifugation
SEC	Size exclusion chromatography
MD	Molecular dynamics
βL	(*S*)-3-(Fmoc-amino)-5-methylhexanoic acid
γL	(R)-Fmoc-4-amino-6-methyl-heptanoic acid
βhL	(*S*)-3-(Fmoc-amino)-6-methylheptanoic acid
γD	(R)-Fmoc-3-amino-hexandioic acid-1-tert-butyl ester
βE	(R)-Fmoc-4-amino-hexandioic acid-1-tert-butyl ester
DIC	Diisoporopylcarbodiimide
HOBT	1-Hydroxybenzotriazole
HOAT	1-Hydroxy-7-azabenzotriazole
TFA	Trifluoroacetic acid
TIS	Triisopropylsilane
DTT	Dithiothreitol
Gnd/HCl	Guanidine hydrochloride
TCEP	Tris(carboxyethyl-)phosphine

Electronic supplementary material The online version of this article (doi:10.1007/s00726-011-0941-z) contains supplementary material, which is available to authorized users.

R. Rezaei Araghi · U. I. M. Gerling · C. D. Cadicamo · B. Koksch (✉)
Institute of Chemistry and Biochemistry, Freie Universität Berlin, Takustraße 3, 14195 Berlin, Germany
e-mail: koksch@chemie.fu-berlin.de

C. Baldauf
CAS-MPG Partner Institute for Computational Biology, SIBS, Shanghai, People's Republic of China
e-mail: baldauf@fhi-berlin.mpg.de

C. Baldauf
Fritz-Haber-Institut der Max-Planck-Gesellschaft, Faradayweg 4-6, 14195 Berlin, Germany

Introduction

Specific helix–helix interaction is fundamental in protein structure assembly, as well as for determining the association between different protein units and domains. Such interactions at molecular level are mediated by a combination of different α-amino acid residue contacts (Anfinsen 1973). This fact has raised the assumption that unnatural residues with comparable contact elements may result in similar helical assemblies. Recent studies on foldamers, unnatural oligomers with predictable conformational propensities (Gellman 1998; Kirshenbaum et al. 1999; Hill et al. 2001; Seebach et al. 2004; Hecht and Huc 2007), have revealed their great potential as versatile tools to engineer helical interfaces in quaternary structures (Cheng and DeGrado 2002; Daniels et al. 2007; Horne et al. 2007; Price et al. 2010; Rezaei Araghi et al. 2010; Rezaei Araghi and Koksch 2011). As a case study, coiled coil motifs represent a unique model system for elucidating principles of helical interaction in both homo- and hetero-assemblies (Lupas and Gruber 2005; Woolfson 2005; Robson Marsden and Kros 2010). α-Helical coiled coil motifs are formed by the binding of two or more α-helical peptides in specific rope-like manner, which is characterized by a heptad repeat denoted "a-b-c-d-e-f-g". The first "a" and fourth "d" positions are predominantly occupied by hydrophobic residues and form the inner-face called the hydrophobic core, while the e and g positions frequently consist of polar or charged residues, packing the electrostatic interface.

The same hydrogen bonding pattern and helix dipole direction of the native α-helical peptides can be found in the alternating $\beta\gamma$-sequences (Karle et al. 1997; Vasudev et al. 2007; Guo et al. 2010). In a recent study, we showed that the successful substitution of an extended sequence of alternating β-and γ-residues in a hetero-tetrameric α-helical coiled coil assembly with retention of global conformation in aqueous solution (Rezaei Araghi et al. 2010). The neighboring α-peptide chains of the $\alpha\beta\gamma$-sequence imposed an α-helical structure on the $\beta\gamma$-foldameric part in order to enable interaction of the hydrophobic and polar interfaces of the hetero-coiled coil assembly. To substantially advance this approach of designing artificial coiled coil motifs, we present in the current report the isosteric substitution of α-residues by sequences of β- and γ-amino acids in GCN4pLI, a tetrameric variant of the yeast transcription factor GCN4 (O'Shea et al. 1989; Harbury et al. 1993). The design of a homo-assembling $\alpha\beta\gamma$-chimeric variant of GCN4pLI leads to inter-helical packing interactions driven locally by extended backbone amino acids. The tetrameric structure of GCN4pLI is an attractive scaffold mainly due to higher interhelical distance and an increased buried surface area compared to dimeric and trimeric structures (Horne et al. 2004; Yadav et al. 2005). This is an important factor in the successful design of engineered coiled coils with unnatural subunits containing extended hydrophobic backbones.

Methods and materials

Peptide synthesis and purification

Peptides were synthesized using an Activo-P11 peptide synthesizer (Activotec GmbH, Cambridge, UK) on a 0.025 mmole scale applying standard Fmoc/tBu chemistry (Fields and Noble 1990) using HOBT/DIC activation. All single couplings were performed with tenfold excess of amino acids and coupling reagents. Manual coupling of β- and γ-amino acids was carried out by HOAT/DIC activation. The molar excess of amino acid and coupling reagents was reduced for β- and γ-residues to twofold for the first and onefold for the second coupling. These couplings were performed manually until completion, as indicated by a negative Kaiser test. Prior to cleavage step, the acetylation of the N-termini was carried out by treatment with 10% acetic anhydride and 10% DIEA in DMF (3 × 10 min). Finally, the resin was treated with a cleavage cocktail composed H_2O:TIS:Thioanisole:DDT: TFA (2.5:2.5:2.5:2.5:90). Purification was carried out by RP-HPLC (Phenomenex_ Luna C8, 10 µl, 250 mm × 21.2 mm) and purity was confirmed by analytical HPLC (Phenomenex_ Luna C8, 5 µl, 250 mm × 4.6 mm). Deionized water and acetonitrile containing 0.1% TFA were used as eluents with a gradient from 5 to 70% acetonitrile over 30 min. All products were identified by high-resolution ESI–MS (Agilent 6210 ESI-TOF mass spectrometer; Agilent Technologies, Santa Clara, CA, USA): GCN4pLI, 13 mg, calcd m/z for $[M + 2H]^{2+}$ was 2,039.6464, found: 2,039.6378; CGG-GCN4pLI, 11.5 mg, calcd m/z for $[M + 2H]^{2+}$ was 2,148.1724, found: 2,148.1721; $\alpha\beta\gamma$-1, 15.5 mg, calcd m/z for $[M + 2H]^{2+}$ was 1,966.6012, found: 1,966.5944; CGG-$\alpha\beta\gamma$1, 7.5 mg, calcd m/z for $[M + 2H]^{2+}$ was 2,075.1273, found: 2,075.1255; $\alpha\beta\gamma$-2, 10.5 mg, calcd m/z for $[M + 2H]^{2+}$ was 1,980.6012, found: 1,980.5911; $\alpha\beta\gamma$-3, 9 mg, calcd m/z for $[M + 2H]^{2+}$ was 1,973.6091, found: 1,973.6021; CGG-$\alpha\beta\gamma$3, 11.5 mg, calcd m/z for $[M + 2H]^{2+}$ was 2,082.1351, found: 2,082.1311; $\alpha\beta\gamma$-4, 10 mg, calcd m/z for $[M + 2H]^{2+}$ was 1,966.6012, found: 1,966.5941; CGG-$\alpha\beta\gamma$4, 14 mg, calcd m/z for $[M + 2H]^{2+}$ was 2,075.1273, found: 2,075.1233.

Circular dichroism spectroscopy

Measurements were carried out with J-810 spectropolarimeter (Jasco GmbH, Gross-Umstadt, Germany), by using

a quartz cuvette (Quartz Suprasil_ cuvettes, Hellma) with 0.1 cm path length, at 20°C (Jasco PTC-348WI peltier thermostat). The spectra were the average of three scans obtained by collecting data in far-UV range 190–240 nm at 0.2 nm intervals, 2 nm bandwidth, and 1 s response time. Ellipticity data in mdeg were converted to conformation parameters, by the following equation: $[\theta] = [\theta]b \times \text{mrw}/10 \times l \times c$, in which $[\theta]b$ is the ellipticity measured in degrees, mrw is the mean residue molecular weight (molecular weight of the peptide divided by the number of amino acid residues), c is the peptide concentration in g mL^{-1}, and l is the optical path length of the cell in cm. The concentration was determined assuming $\varepsilon_{274\ nm} =$ 1,400 M^{-1} cm^{-1} for tyrosine. Peptide stock solutions were stored occasionally at −22°C and diluted to an appropriate concentration with buffer before use. Melting curves were recorded using the signal at 222 nm applying a heating rate of 3 K/min from 20 to 100°C. Each experiment was carried out in triplicate, and both the baseline corrected spectra and the melting curves were averaged. The details of the conditions were as follows: (a) the self-assemblies (Fig. 4): 150 μM total peptide concentration, 50 mM phosphate buffer pH 7.4; (b) the hetero-assemblies (Fig. 5): 50 μM total peptide concentration, 50 mM phosphate buffer pH 7.4, 2.5 M Gnd/HCl.

Size-exclusion chromatography

Size-exclusion chromatography was accomplished with a VWR-Hitachi Elite LaChrome system (Pump l-2130, UV Detector L-2400, VWR, Darmstadt, Germany) equipped with a Superdex 75 PC 3.2/30 column from Amersham Biosciences. Elution buffer was sodium phosphate (100 mM, pH 7.4) and the flow rate was 0.025 mL min^{-1}. Peptide absorbance was registered at 220 nm. For molecular-weight calibration, the Gel Filtration Calibration Kit LMW form GE Healthcare Life Sciences was used. The retention times are corrected with internal and external references. Anthranilic acid labeled Gly is used as internal reference. GCN4-p1, GCN4-pII, and GCN4-pLI were applied as references for dimeric, trimeric and tetrameric coiled coils (Harbury et al. 1993).

Analytical ultracentrifugation

The measurements were performed on a XL-I (Beckman-Coulter, Palo Alto, CA, USA) ultracentrifuge at 293 K using standard 12 mm double sector center pieces. Sedimentation velocity (SV) experiments were conducted applying the UV–Vis absorption optics at 273 nm at 60,000 rpm [RCF value of 2,900,000 ($\times g$), where the radial distance from the axis of the rotor (r) is 72 mm] and overall peptide concentration of 150 μM. Prior to AUC analysis, the proteins were extensively dialysed against 50 mM phosphate buffer (pH 7.6) using a Spectra-Por®Membran (MWCO; Carl Roth GmbH) to ensure absence of salt. The samples were diluted by 50 mM phosphate buffer at pH 7.6. The densities of buffer ($\rho = 1.005555$ g ml^{-1} at 25°C) and samples were determined in a density oscillation tube (DMA 5000, Anton Paar, Graz) and the partial specific volume of the samples was determined to be 0.895 ml g^{-1}. Buffer viscosity ($\eta = 0.0093737$ P at 25°C) were calculated using the freeware program SEDNTERP (Lebowitz et al. 2002). The sedimentation velocity data were evaluated using the program SEDFIT (Schuck 2000) yielding the sedimentation coefficient distributions. The sedimentation equilibrium experiments were obtained at a temperature of 293 K at rotor speeds of 30,000 rpm (723,816×g), 35,000 rpm (985,194×g), 40,000 rpm (1,286,784×g) and 45,000 rpm (1,628,586×g) at varying concentrations from 50 to 500 μM. Scanning wavelengths of 269, 273 and 285 nm were used. Apparent weight average molar masses, $M_{w,app}$ (Figs. S1, S2) were determined using the model independent MSTAR procedure of Harding and Coelfen.

The disulfide exchange assay

The homo-disulfide-bonded species preparation

The peptide (10 mg) was dissolved in DMF:H_2O solution (total volume of 1.5–2 ml) and stirred overnight at room temperature. The mixture was purified directly by HPLC. The fractions containing the homo-species were collected and lyophilized to obtain: CGG-GCN4pLI/CGG-GCN4pLI, 8 mg, calcd m/z for $[M + 6H]^{6+}$ was 1,418.1123, found: 1,418.1089; CGG-αβγ1/CGG-αβγ1, 6.5 mg, calcd m/z for $[M + 6H]^{6+}$ was 1,369.4155, found: 1,369.4051; CGG-αβγ2/CGG-αβγ2, 7.5 mg, calcd m/z for $[M + 6H]^{6+}$ was 1,378.7488, found: 1,378.69909; CGG-αβγ3/CGG-αβγ3, 6.8 mg, calcd m/z for $[M + 6H]^{6+}$ was 1,374.0874, found: 1,374.0676; CGG-αβγ4/CGG-αβγ4, 8.5 mg, calcd m/z for $[M + 2H]^{2+}$ was 1,369.4155, found: 1,369.4001.

The hetero-disulfide-bonded species preparation

A 1:1 molar ratio of both peptides (in total about 10 mg) was dissolved in 2:1 DMF/H_2O solution (total volume of 1.5–2 ml) and stirred overnight at room temperature. The mixture was purified directly by HPLC. The fractions containing the homo-species were collected and lyophilized to obtain: CGG-GCN4pLI/CGG-αβγ1, 6.5 mg, calcd m/z for $[M + 6H]^{6+}$ was 1,393.7639, found: 1,393.7431; CGG-GCN4pLI/CGG-αβγ2, 5.0 mg, calcd m/z for $[M + 6H]^{6+}$ was 1,403.0972, found: 1,403.0051; CGG-GCN4pLI/CGG-αβγ3, 7.5 mg, calcd m/z for $[M + 6H]^{6+}$

was 1,396.0998, found: 1,396.1909; CGG-GCN4pLI/CGG-$\alpha\beta\gamma$4, 7.5 mg, calcd m/z for $[M + 6H]^{6+}$ was 1,374.0874, found: 1,374.0676; CGG-$\alpha\beta\gamma$4/CGG-$\alpha\beta\gamma$4, 8.5 mg, calcd m/z for $[M + 6H]^{6+}$ was 1,393.7639, found: 1,393.7699.

Hetero disulfide-bonded association

The experiments were performed as described by (Yoder and Kumar 2006). The purified samples of homo-species CGG-GCN4pLI/CGG-GCN4pLI and CGG-X/CGG-X (where X is $\alpha\beta\gamma$1, $\alpha\beta\gamma$2, $\alpha\beta\gamma$3, and $\alpha\beta\gamma$4 in each set of experiment) in 1:1 molar ratio and 100 µM total concentration were incubated in redox buffer (50 mM phosphate buffer, pH 7.8, supplemented with 500 µM reduced glutathione and 125 µM oxidized glutathione) in the presence of 0.1 equiv. TCEP at 20°C under argon. The progress of the reaction was monitored over the course of 33 h by removing a 300 µL aliquot, quenching the reaction with acetic acid (to a 10% v/v final concentration of acetic acid) and injecting the aliquot on a reverse-phase HPLC (analytical C18 column) a gradient of acetonitrile/water in the presence of 0.1% trifluoroacetic acid.

Hetero disulfide-bonded dissociation

The reverse equilibration was performed by incubating 100 µM purified CGG-GCN4pLI/CGG-X (where X is $\alpha\beta\gamma$1, $\alpha\beta\gamma$2, $\alpha\beta\gamma$3, and $\alpha\beta\gamma$4 in each set of experiment) in the same redox buffer and at 20°C under argon. The progress of the reaction was monitored over the course of 33 h using the same method as described above. The disulfide exchange reached equilibrium within 24 h for reactions in both directions. The disulfide-bridge rearrangement is catalyzed by a very small amount (0.1 equiv.) of the reductant TCEP in order to create free thiol peptide and therefore facilitating the initiation of the disulfide-bridge exchange (Yoder and Kumar 2006).

Modeling and molecular dynamic simulations

Modeling of the GCN4pLI and the $\alpha\beta\gamma$ chimeras is based on the X-ray structure 1GCL (Harbury et al. 1993) to which missing C terminal residues were added. In case of the variants $\alpha\beta\gamma$-1 to $\alpha\beta\gamma$-4, the residues Leu_9, Glu_{10}, Glu_{11}, Ile_{12}, Leu_{13}, Ser_{14} were deleted and the $\beta\gamma$-segments were added into the sequence in an α-helix like conformation as described in (Baldauf et al. 2006). Exemplary structures of the tetrameric GCN4pLI and the variant $\alpha\beta\gamma$-1 can be seen in Fig. 2. All MD simulations and part of the analysis were carried out with the Gromacs suite of programs (version 4.0.5) (Hess et al. 2008) employing the Gromos 53a6 force field (Oostenbrink et al. 2004). The proteins were solvated in dodecahedral boxes with SPC water molecules and periodic boundary conditions were applied. The typical protonation states at pH 7 were chosen for ionizable groups of the peptide. The necessary amount of counter-ions (Cl^- and Na^+) was added to ensure a neutral system and salt concentration 0.1 mol/l. Prior to free MD simulations, steepest descent energy minimizations and position restrained MD simulations with heavy atom positions restrained with a harmonic potential using a spring constant of 1,000 kJ/mol nm^2 (100 ps) were performed. Temperature (300 K) and pressure (1 bar) were coupled to a Nosé–Hoover thermostat (Nosé 1984; Hoover 1985) and a Parrinello–Rahman barostat (Parrinello and Rahman 1981; Nosé and Klein 1983), using time constants of 0.1 and 1 ps, respectively. Non-bonded interactions were considered within a cut-off of 1 nm, and long-range electrostatic interactions were calculated using the Particle-Mesh-Ewald algorithm (Darden et al. 1993). Constraints were applied by the LINCS algorithm (Hess et al. 1997). A time step of 2 fs was used for integration. The Gromos 53a6 topologies of the β- and γ-amino acids are available from the authors upon request.

Results and discussions

Design

A clear α-helical coiled coil structure of GCN4pLI has emerged from the crystal structure (Harbury et al. 1993), which allows a structure-based design of $\alpha\beta\gamma$-chimeric helical interfaces. Based on the principle of "equal backbone atoms" (Banerjee and Balaram 1997; Karle et al. 1997; Baldauf et al. 2006), Leu^9, Glu^{10}, and Glu^{11} were replaced by βLeu^9 and γAsp^{10} while Ile^{12}, Leu^{13}, and Ser^{14} were substituted by βIle^{11} and γLeu^{12} in the first $\alpha\beta\gamma$-chimeric variant of GCN4pLI ($\alpha\beta\gamma$-1). Each modification of this type is adding three CH_2 units into the backbone and omits one peptide bond. Furthermore, as we only make use of ω-substituted amino acids, one side chain from the wild type sequence (Fig. 1a, b) is omitted as well. In selecting which side chains to preserve and which to omit, we applied the following argument based on the molecular modeling and simulation (Figs. 2, 3). We considered the preservation of original side chains of the residues in crucial interhelical domains, especially those at hydrophobic sites ($Leu^9 \rightarrow \beta Leu^9$ and $Ile^{12} \rightarrow \beta Ile^{11}$), therefore the omitted side chains were chosen to be on the solvent-exposed region (Glu^{11} and Ser^{14}) in order not to interfere with helix–helix interactions.

The partial decline in stability of the entire quaternary structure can be anticipated due to the loss of one peptide bond and therewith one H-bond donor and one H-bond acceptor per $\alpha \rightarrow \beta\gamma$ isosteric substitution. However, we

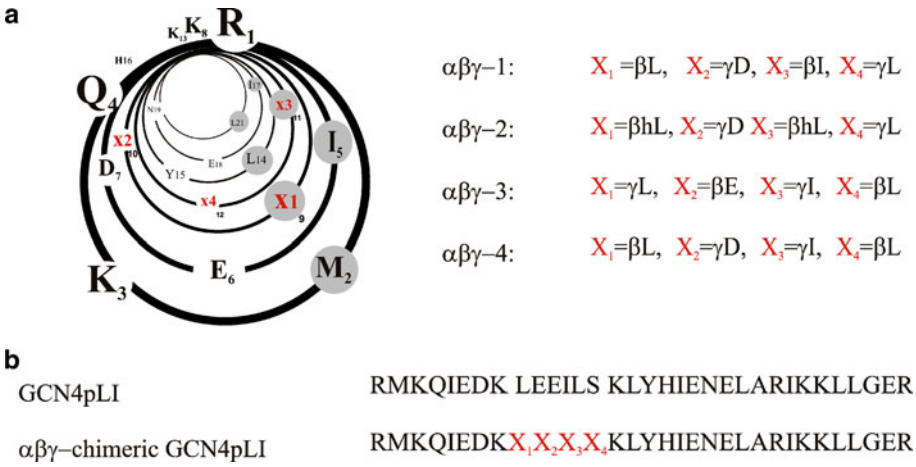

Fig. 1 **a** The helical representation of 21 N-terminal amino acids in $\alpha\beta\gamma$-chimeric variants of GCN4pLI. The amino acids at the hydrophobic core are highlighted in *grey*. The substituted β - and γ-amino acids in the $\alpha\beta\gamma$-chimeric sequences are designated in X1–X4. **b** The primary structure of the GCN4pLI and general sequence of $\alpha\beta\gamma$-chimera

hypothesize that the loss of this peptide bond is not sufficient to cause considerable disorder in the entire modified interhelical domain, unless it is accompanied by other perturbative structural consequences such as disruption in local packing or conformational chaos due to further loss of H-bonds. The packing of the hydrophobic core (Fig. 3b) is a key element in determining the stability of coiled coils; therefore modifications leading to non-sufficient van der Waals interactions at the interior part of helix-bundle fail to adopt suitably this particular folding motif (Faham et al. 2004; Zhang et al. 2009). This may arise from the fact that the increased hydrophobic surface area provided by extended backbone amino acids at the core of the corresponding helix-bundle is not completely inaccessible to the surrounding aqueous solution. This design hypothesis can be probed by a series of control chimeric peptides; $\alpha\beta\gamma$-2, $\alpha\beta\gamma$-3, and $\alpha\beta\gamma$-4. In $\alpha\beta\gamma$-2, both β-residues at the hydrophobic core of $\alpha\beta\gamma$-1 are changed to β-homoleucine, which are expected to provide a close-packing at the interior part of the corresponding helix bundle due to suitably long side chains. An oppositely arranged sequence of $\beta\gamma$ in the $\alpha\beta\gamma$-3 creates an exclusive hydrophobic packing between γ-amino acids and consequently increases the solvent accessible interhelical surface compared to $\alpha\beta\gamma$-1. Finally, the importance of specific intrahelical H-bonding which is provided by a distinct alternating sequence of β- and γ-amino acids can be examined by breaking this alternation in $\alpha\beta\gamma$-4.

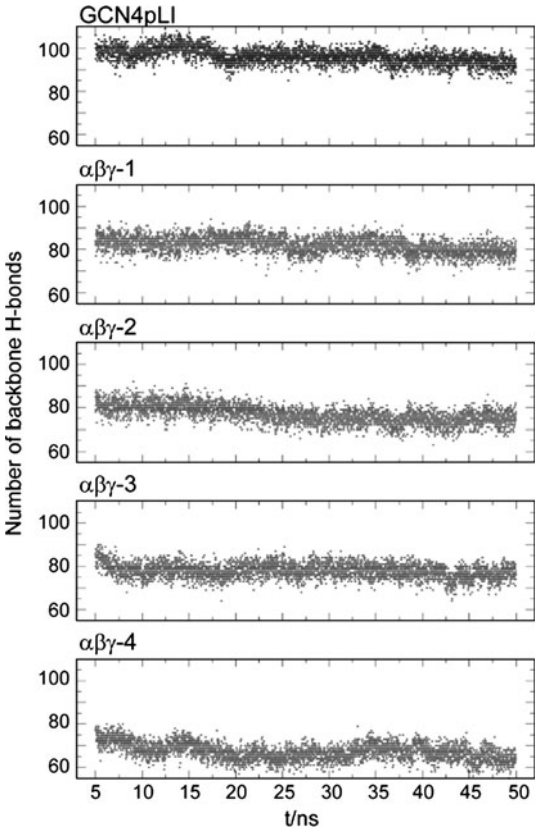

Fig. 2 Molecular dynamics simulations for the homo-tetramers GCN4pLI, $\alpha\beta\gamma$-1, $\alpha\beta\gamma$-2, $\alpha\beta\gamma$-3, and $\alpha\beta\gamma$-4. The number of backbone H-bonds monitored during the simulation time

MD simulations

The molecular dynamics simulations which have been performed on GCN4pLI as well as on the $\alpha\beta\gamma$ variants, confirm a partial perturbation in H-bonding pattern of the entire quaternary structure due to the loss of one peptide bond per $\alpha \rightarrow \beta\gamma$ substitution (Fig. 2). For GCN4pLI in average 95 backbone H-bonds were monitored during 50 ns of MD simulations. The $\beta\gamma$ substitutions of $\alpha\beta\gamma$-1, $\alpha\beta\gamma$-2, and $\alpha\beta\gamma$-3 reduce this to about 80 to 85 backbone H-bonds, due to the loss of one peptide bond and due to non-ideal arrangement of donor and acceptor pairs between the α-sequences and the $\beta\gamma$-foldameric part. The variant $\alpha\beta\gamma$-4 disrupts H-bonding even more and results in average in only about 65 H-bonds. On the other hand, the representative MD snapshots in Fig. 3 highlight that; the observed perfect packing of the hydrophobic residues for GCN4pLI is sufficiently well reproduced by the variants

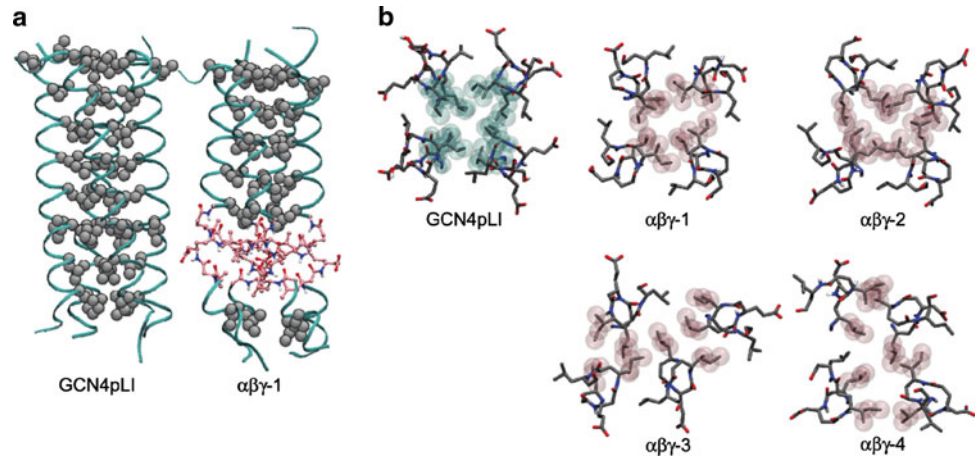

Fig. 3 Representative structures from the MD trajectories. **a** The tetramer of GCN4pLI as simulated, the helix is shown as a ribbon, the side chain carbons of the aliphatic residues Leu and Ile are drawn as *grey* van der Waals spheres. Same drawing rules were used for $\alpha\beta\gamma$-1, the $\beta\gamma$ part is highlighted as CPK model. **b** Only the residues Leu_9, Glu_{10}, Glu_{11}, Ile_{12}, Leu_{13}, and Ser_{14} are shown for GCN4pLI, side chain carbons contributing to the hydrophobic core are highlighted by transparent van der Waals spheres. The substituted $\beta\gamma$ segments are shown for $\alpha\beta\gamma$-1, $\alpha\beta\gamma$-2, $\alpha\beta\gamma$-3, and $\alpha\beta\gamma$-4, carbons of the hydrophobic core are again highlighted by transparent van der Waals spheres

$\alpha\beta\gamma$-1 and $\alpha\beta\gamma$-2. As expected, the packing for $\alpha\beta\gamma$-3 and $\alpha\beta\gamma$-4 is far less ideal and a substantially reduced stability can be expected.

Structural characterization

Circular dichroism spectroscopy (CD) and analytical ultracentrifugation (AU) were used to investigate the impact of the applied modification on the ability of $\alpha\beta\gamma$-1 to form helical quaternary structure in aqueous solution. Variant $\alpha\beta\gamma$-1 exhibits a considerable degree of α-helicity at 150 μM by presenting the canonical CD minimum at 222 nm (Fig. 4a). The AU results of $\alpha\beta\gamma$-1 indicates a single species with molecular weight expected for a four helix-bundle (Table 1 and Supporting Information). This is remarkable, because it shows that the isosteric replacement of $\beta\gamma$-foldameric pattern does result in the same energetically preferred tetrameric association state as for GCN4pLI.

Variable temperature CD measurement showed a melting temperature for $\alpha\beta\gamma$-1 of 72°C, somewhat lower than the T_m value for GCN4pLI which melts above 100°C (Fig. 4b).

As with $\alpha\beta\gamma$-1, $\alpha\beta\gamma$-2 represent the tetrameric oligomerization state (Table 1, and the Supporting Information). Interestingly, the CD spectrum obtained for $\alpha\beta\gamma$-2 has more intense minima compared to $\alpha\beta\gamma$-1 and the T_m value is

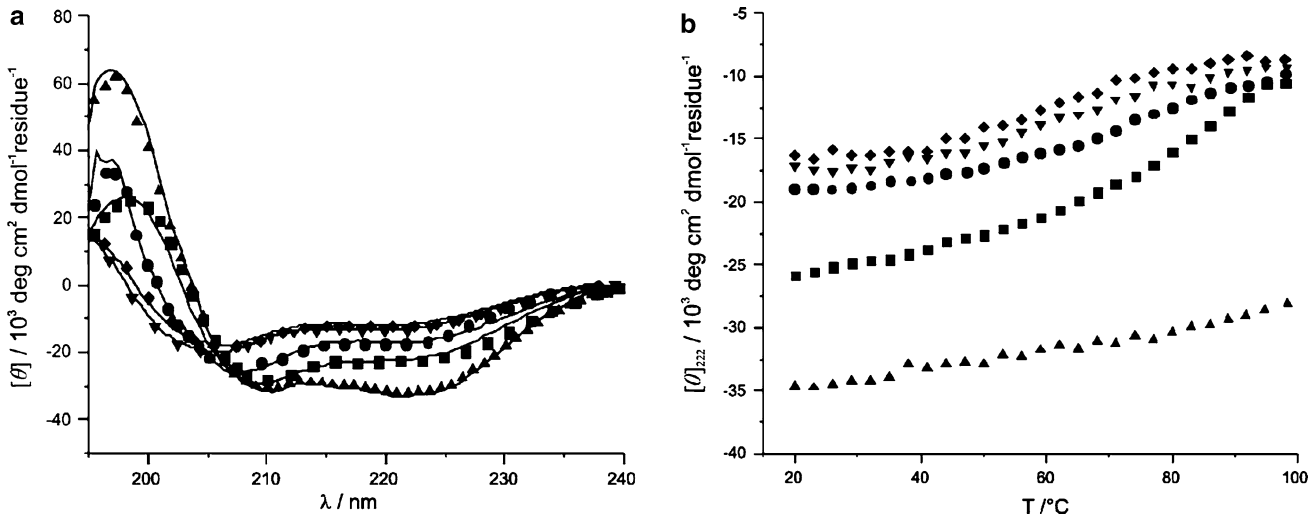

Fig. 4 **a** CD spectra, **b** thermal denaturation of self-assembled GCN4pLI *triangle*, $\alpha\beta\gamma$1 *circle*, $\alpha\beta\gamma$2 *square*, $\alpha\beta\gamma$3 *inverted triangle*, $\alpha\beta\gamma$4 *diamond*, 150 μM peptide concentration in phosphate buffer 50 mM pH 7.4

Table 1 Biophysical data for GCN4-derived peptide and $\alpha\beta\gamma$-variants

Peptides	$[\theta]_{222}$ deg cm^2 dmol^{-1}[a]	$N^{b}_{olig.}$
GCN4pLI	−35,700	4[c]
$\alpha\beta\gamma$-1	−26,400	4[d]
$\alpha\beta\gamma$-2	−19,200	4[d]
$\alpha\beta\gamma$-3	−17,100	7[e]
$\alpha\beta\gamma$-4	−15,500	6/7[e]

[a] For experimental details please see "Circular dichroism" section and full spectra in Fig. 4

[b] Apparent oligomerization state of the GCN4-derived peptide and $\alpha\beta\gamma$-variants in solution

[c] Referring to (Harbury et al. 1993)

[d] The oligomerization state of these species was confirmed with both AUC and SEC (please see the supporting information)

[e] Referring to analytical ultracentrifugation results (please see the Supporting Information)

significantly increased to 83°C (Fig. 4a, b). The results obtained by regular and variable temperature CD measurement support the hypothesis, that enhancement in packing within the hydrophobic core can compensate for the loss of thermal stability due to the backbone modification. The interlocking of the suitably long *iso*-pentyl side chains allow the helix–helix interfaces to come into closer contact, simultaneously increasing their van der Waals interactions likely through side chain-side chain and even side chain-backbone hydrophobic contact between the neighboring helices.

If the quaternary structure stability is recovered due to well-buried hydrophobic surface area, then conversely it can be expected that an increase in solvent-exposed surface from the interior part of the helix-bundle result in loss of stability. We therefore prepared and tested another mutant, $\alpha\beta\gamma$-3 (Fig. 1a, b). The ellipticity at 222 nm of $\alpha\beta\gamma$-3 is less intense and slightly blue-shifted, and the T_m value (62°C) is significantly reduced compared to $\alpha\beta\gamma$-1 (72°C) and $\alpha\beta\gamma$-2 (83°C). These results suggest a general decline in stability of the quaternary structure, as we were expecting from modeling. Furthermore, the AU results of $\alpha\beta\gamma$-3 indicate higher order oligomers (heptamers). Apparently, the large solvent accessible hydrophobic surface area of the γ-residues induces higher oligomerization states which allows the burial of surface from the surrounding solvent. Another plausible explanation might be a mismatched "hole-to-hole" instead of classical "knob-into-hole" interaction by γ-residues at the hydrophobic core, which results in the helical packing complications.

Additionally, we generated $\alpha\beta\gamma$-4 by introducing one β- and one γ-amino acid within the hydrophobic core with retention of the side chain functionality in $\alpha\beta\gamma$-1 (Fig. 1a, b). $\alpha\beta\gamma$-4 is the least stable variant among the four with a melting temperature of 59°C (Fig. 4b). The explanation can be taken again from the modeling and simulation, with a loose packing of the hydrophobic side chains of the $\beta\gamma$ part (Fig. 3b). The AU results are consistent with the presence of non-specific higher order oligomers (Table 1). The special $\beta\gamma\gamma\beta$ substitution pattern in $\alpha\beta\gamma$-4 breaks with the pattern of $\beta\gamma$ segment substitution employed in other variants. As a result, the H-bonding pattern within the $\beta\gamma$ stretch as well as to the flanking α-residues is substantially disturbed. Variant $\alpha\beta\gamma$-4 is the species with the least backbone H-bonds in the MD simulation (Fig. 2). This is likely an important factor in the destabilization of the quaternary structure.

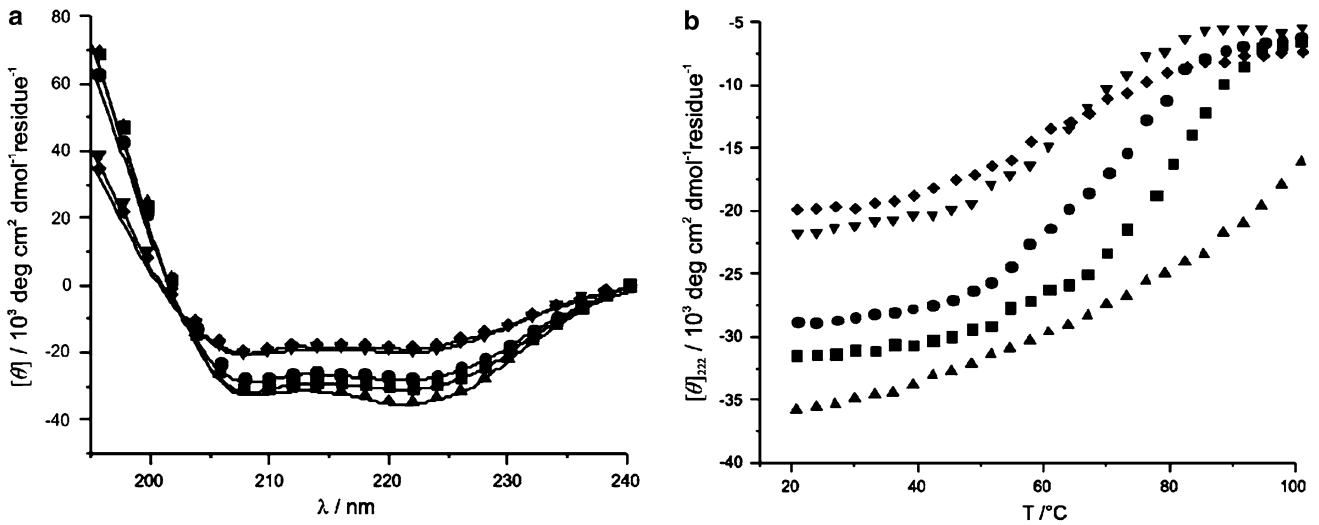

Fig. 5 **a** CD spectra, **b** thermal denaturation of hetero-oxidized species of CGG-GCN4pLI/CGG-$\alpha\beta\gamma$1 *circle*, CGG-GCN4pLI/CGG-$\alpha\beta\gamma$2 *square*, CGG-GCN4pLI/CGG-$\alpha\beta\gamma$3 *inverted triangle*, CGG-GCN4pLI/CGG-$\alpha\beta\gamma$4 *diamond*, and the homo-oxidized CGG-GCN4pLI/CGG-GCN4pLI *triangle*, 50 μM peptide concentration in phosphate buffer 50 mM pH 7.4 containing 2.5 M GndHCl

The $\alpha\beta\gamma$-1 and $\alpha\beta\gamma$-2 variants exhibit the very same biophysical behavior as the GCN4pLI system. This fact may favor their association with the wild type sequence, which would result in the formation of hetero-species. The hetero-assembly of the wild type with $\alpha\beta\gamma$-chimeric variants was forced by close contact due to disulfide-bridges between two species. Derivatives of all studied sequences were prepared by appending cysteine to the N terminus via a flexible Gly–Gly linker. The hetero-species of hetero-oxidized1, hetero-oxidized2, hetero-oxidized3, and hetero-oxidized4 were prepared by air-oxidation of CGG-GCN4pLI with CGG$\alpha\beta\gamma$-1, CGG$\alpha\beta\gamma$-2, CGG$\alpha\beta\gamma$-3 and CGG$\alpha\beta\gamma$-4 respectively. The SEC results reveal the appearance of tetrameric assemblies for hetero-oxidized1 and hetero-oxidized2 but multiple higher order species for hetero-oxidized3 and hetero-oxidized4 (Supporting Information). The CD spectra of all hetero-species represent significant α-helicity, however, the differences in magnitude of the spectra and T_m values reflect the difference in the structural stability of the hetero quaternary structures (Fig. 5a, b).

Following the same trend observed in stability of homo-assembled $\alpha\beta\gamma$-chimeric variants, the hetero-association of the $\alpha\beta\gamma$-2 with GCN4pLI distinctly results not only in a similar oligomerization state to GCN4pLI, but also in significant thermal stability. Despite the possible differences in packing geometry of the quaternary structure of hetero-2, these results suggest that the $\beta\gamma$-foldameric sequence in general and the iso-pentyl side chains of β-homoleucine residues in particular experience a similar compact interaction environment as exists in GCN4pLI. The close hydrophobic contact of β-homoleucine residues to the hydrophobic side-chains and backbone atoms of the neighboring α-helices in the corresponding tetrameric assembly provide for the condensed packing. It is likely that such hydrophobic interactions compensate for the entropic penalty associated with $\alpha \rightarrow \beta\gamma$ replacement in $\alpha\beta\gamma$ variants of GCN4pLI.

An interest in determining how differences in side-chain packing influence the pairing specificity of the $\alpha\beta\gamma$-variants in solution motivated the next part of our investigations. Therefore, a disulfide bridge exchange assay was performed, which uses the relative populations of disulfide-bonded species at equilibrium, as an indicator of thermodynamic stability (O'Shea et al. 1989; Bilgicer et al. 2001; Yoder and Kumar 2006; Qiu et al. 2006). The preference for hetero-structure association is studied in a redox experiment in which the homo-oxidized CGG-$\alpha\beta\gamma$1 is equilibrated with homo-oxidized CGG-GCN4pLI in a redox buffer that facilitates disulfide bridge exchange (Fig. 6a). A set of control experiments was performed under the same conditions in the presence of homo-oxidized2, homo-oxidized3, homo-oxidized4 species which were prepared by air-oxidation of the CGG-$\alpha\beta\gamma$2, CGG-$\alpha\beta\gamma$3 and CGG-$\alpha\beta\gamma$4, respectively (Fig. 6b–d). All experiments reveal the dominant population of homo-bridged CGG-GCN4pLI, which is not surprising due to the ideal packing of the helix-bundle in GCN4pLI. However, a small but significant amount of hetero-oxidized of CGG-GCN4pLI/CGG-$\alpha\beta\gamma$1 is detected at equilibrium condition and characterized by HPLC and ESI-TOF mass spectrometry. Interestingly, when the same experiment was conducted with the homo-assemblies of CGG-GCN4pLI and CGG-$\alpha\beta\gamma$2, a larger population of the respective hetero species was obtained (Fig. 6b), while the incubation of the homo-oxidized variants CGG-$\alpha\beta\gamma$3 and CGG-$\alpha\beta\gamma$4 with homo-oxidized CGG-GCN4pLI results in either negligible

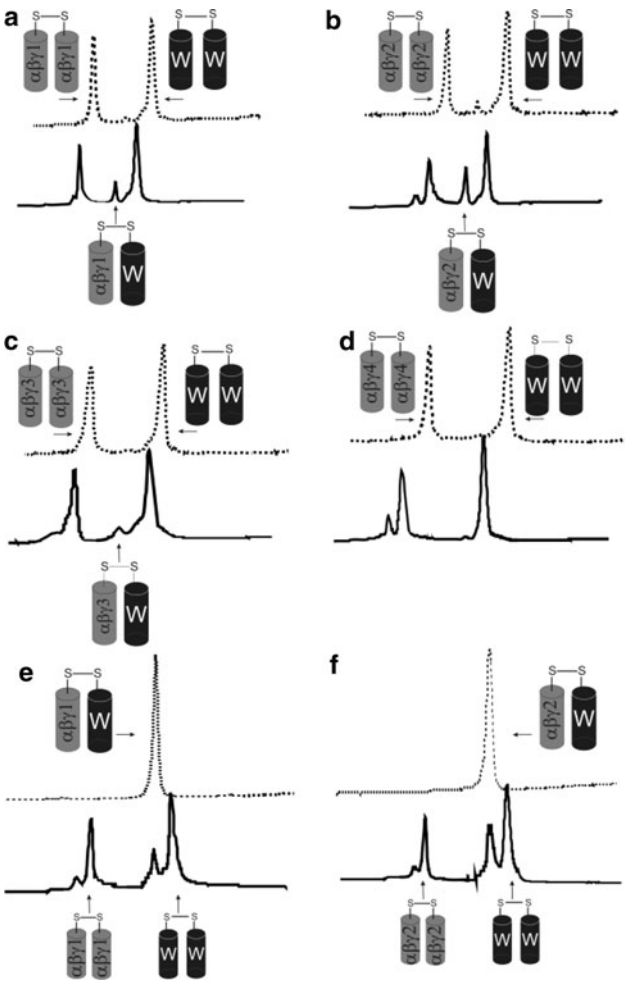

Fig. 6 Equilibrium disulfide-exchange assay for homo-species of GCN4pLI-GCN4pLI in presence of **a** homo-oxidized1, **b** homo-oxidized2, **c** homo-oxidized3 and **d** homo-oxidized4. Equilibrium disulfide-exchange assay for hetero-species of **e** CGG-GCN4pLI/CGG-$\alpha\beta\gamma$1 and **f** CGG-GCN4pLI/CGG-$\alpha\beta\gamma$2. The chromatograms are presented after 5 min (*dash line*) and 24 h (*solid line*). Small peaks eluting before homo-oxidized species are the disulfide-bonded product of glutathione to the corresponding monomers

or undetectable amounts of the respective hetero species (Fig. 6c, d). These results highlight again the native-like biophysical behaviors of the variants $\alpha\beta\gamma$-1 and in particular $\alpha\beta\gamma$-2. The considerable population of the hetero species, as observed especially for the CGG-GCN4pLI/CCG-$\alpha\beta\gamma$-2 system, is due to the extent of interhelical packing. In contrast, the optimal side chain orientation in CGG-$\alpha\beta\gamma$3 and CGG-$\alpha\beta\gamma$4 appears to be the main factor disfavoring their hetero-assembly with GCN4pLI. It is known that the disulfide bond formation under redox condition is thermodynamically coupled to the extent of association of the peptides. Therefore the maintenance or restoration of disulfide-bridged hetero-oxidized species demonstrates the affinity between two peptides. This could be best realized by CGG-$\alpha\beta\gamma$-2.

The dissociation control experiment confirms these results in another way. The incubation of the pre-formed hetero-oxidized species in redox buffer provides opportunity for the reduction and dissociation of the energetically disfavored disulfide-bridged species. Surprisingly, the disulfide bridge rearrangement is only performed partially and incompletely for both hetero-oxidized1 and hetero-oxidized2 while the amount of non-dissociated hetero-species are considerable in the latter case (Fig. 6e, f). In light of our observation, there is a close correlation between the pairing affinity and the more optimal side chain packing at the helical interfaces. The relatively high stability of the hetero-oxidized species under redox condition suggests a similar compact helix–helix interaction in CGG-GCN4pLI/CGG-$\alpha\beta\gamma$1 and more specifically in CGG-GCN4pLI/CGG-$\alpha\beta\gamma$2 to that observed in the classical packing of native coiled coil motif.

Conclusion

We propose alternating patterns of β- and γ-amino acids as a novel design element within α-helical constructs. Our systematic study shows that isosteric substitution of α-amino acids with specific patterns of β- and γ-amino acids in the biologically derived GCN4pLI sequence, adhering to the principle of "equal backbone atoms", has a significant impact on its self-assembly. The significant differences in thermodynamic stability and specificity of these self-assembled quaternary structures reveals the disruptive structural consequences which are associated with certain $\alpha \rightarrow \beta\gamma$ backbone modifications, and these in turn influence the physical behavior of the chimeric sequences relative to the original α-sequences. As in a native α-helical coiled coil, the van der Waals interactions at the hydrophobic interface of the helical coiled coils are critically involved in the association of the $\alpha\beta\gamma$-chimeric sequences with either other chimeras or the native α-peptide. In view of the above described theoretical and experimental observations, we conclude that such interactions are able to compensate to some extent for the entropic penalty incurred by the increase in conformational flexibility of the backbone. Acknowledging that, many different strategies can be offered to reinforce the stability of the modified structures. This study shows that limiting the solvent accessibility of the hydrophobic surface and optimizing the steric bulk/length of the aliphatic side chains within the hydrophobic core are examples of these strategies to provide for close residue contacts and appropriate packing parameters that result in greater thermodynamic stability. In the light of the current strong attempts in modifications applied to a variety of helix–helix interaction domains, we believe that these results should be of general interest, as they highlight the great potential of the $\beta\gamma$ motif for generation of artificial helices as well as the structural limits behind such backbone modification.

Acknowledgments This work was funded by Freie Universität Berlin. R. Rezaei Araghi is grateful for the scholarship from Dahlem Reseach School. We thank Dr. Allison Berger for proof reading.

Conflict of interest The authors declare that they have no conflict of interest.

References

Anfinsen CB (1973) Principles that govern the folding of protein chains. Science 181:223–230

Baldauf C, Günther R, Hofmann H-J (2006) Helix formation in α, γ- and β, γ-hybrid peptides: theoretical insights into mimicry of α- and β-peptides. J Org Chem 71:1200–1208

Banerjee A, Balaram P (1997) Stereochemistry of peptides and polypeptides containing omega amino acids. Curr Sci India 73:1067–1077

Bilgicer B, Xing X, Kumar K (2001) Programmed self-sorting of coiled coils with leucine and hexafluoroleucine cores. J Am Chem Soc 123:11815–11816

Cheng RP, DeGrado WF (2002) Long-range interactions stabilize the fold of a non-natural oligomer. J Am Chem Soc 124:11564–11565

Daniels DS, Petersson EJ, Qiu JX, Schepartz A (2007) High-resolution structure of a β-peptide bundle. J Am Chem Soc 129:1532–1533

Darden T, York D, Pedersen L (1993) Particle mesh Ewald: an N.log(N) method for Ewald sums in large systems. J Chem Phys 98:10089–10092

Faham S, Yang D, Bare E, Yohannan S, Whitelegge JP, Bowie JU (2004) Side-chain contributions to membrane protein structure and stability. J Mol Biol 335:297–305

Fields GB, Noble RL (1990) Solid phase peptide synthesis utilizing 9-fluorenylmethoxycarbonyl amino acids. Int J Pept Protein Res 35:161–214

Gellman SH (1998) Foldamers: a manifesto. Acc Chem Res 31:173–180

Guo L, Almeida AM, Zhang W, Reidenbach AG, Choi SH, Guzei IA, Gellman SH (2010) Helix formation in preorganized β/γ-peptide

foldamers: hydrogen-bond analogy to the α-helix without α-amino acid residues. J Am Chem Soc 132:7868–7869
Harbury PB, Zhang T, Kim PS, Alber T (1993) A switch between two-, three-, and four-stranded coiled coils in GCN4 leucine zipper mutants. Science 262:1401–1407
Hecht S, Huc I (2007) Foldamers. Wiley-VCH, Weinheim
Hess B, Bekker H, Berendsen HJC, Fraaije JGEM (1997) LINCS: a linear constraint solver for molecular simulations. J Comput Chem 18:1463–1472
Hess B, Kutzner C, van der Spoel D, Lindahl E (2008) GROMACS 4: algorithms for highly efficient, load-balanced, and scalable molecular simulation. J Chem Theory Comput 4:435–447
Hill DJ, Mio MJ, Prince RB, Hughes TS, Moore JS (2001) A field guide to foldamers. Chem Rev 101:3893–4012
Hoover WG (1985) Canonical dynamics: equilibrium phase-space distributions. Phys Rev A 31:1695–1697
Horne WS, Yadav MK, Stout CD, Ghadiri MR (2004) Heterocyclic peptide backbone modifications in an α-helical coiled coil. J Am Chem Soc 126:15366–15367
Horne WS, Price JL, Keck JL, Gellman SH (2007) Helix bundle quaternary structure from α/β-peptide foldamers. J Am Chem Soc 129:4178–4180
Karle IL, Pramanik A, Banerjee A, Bhattacharjya S, Balaram P (1997) ω-Amino acids in peptide design. Crystal structures and solution conformations of peptide helices containing a b-alanyl-g-aminobutyryl segment. J Am Chem Soc 119:9087–9095
Kirshenbaum K, Zuckermann RN, Dill KA (1999) Designing polymers that mimic biomolecules. Curr Opin Struct Biol 9:530–535
Lebowitz J, Lewis MS, Schuck P (2002) Modern analytical ultracentrifugation in protein science: a tutorial review. Protein Sci 11:2067–2079
Lupas AN, Gruber M (2005) The structure of α-helical coiled coils. Adv Protein Chem 70:37–38
Nosé S (1984) A molecular dynamics method for simulations in the canonical ensemble. Mol phys 52:255–268
Nosé S, Klein ML (1983) Constant pressure molecular dynamics for molecular systems. Mol phys 50:1055–1076
Oostenbrink C, Villa A, Mark AE, Van Gunsteren WF (2004) A biomolecular force field based on the free enthalpy of hydration and solvation: the GROMOS force-field parameter sets 53A5 and 53A6. J Comput Chem 25:1656–1676
O'Shea EK, Rutkowski R, Kim PS (1989a) Evidence that the leucine zipper is a coiled coil. Science 243:538–542
O'Shea EK, Rutkowski R, Stafford WF, Kim PS (1989b) Preferential heterodimer formation by isolated leucine zippers from fos and jun. Science 245:646–648
Parrinello M, Rahman A (1981) Polymorphic transitions in single crystals: a new molecular dynamics method. J Appl Phys 52:7182–7190
Price JL, Horne WS, Gellman SH (2010) Structural consequences of β-amino acid preorganization in a self-assembling α/β-peptide: fundamental studies of foldameric helix bundles. J Am Chem Soc 132:12378–12387
Qiu JX, Petersson EJ, Matthews EE, Schepartz A (2006) Toward β-amino acid proteins: a cooperatively folded b-peptide quaternary structure. J Am Chem Soc 128:11338–11339
Rezaei Araghi R, Koksch B (2011) A helix-forming αβγ-chimeric peptide with catalytic activity: a hybrid peptide ligase. Chem Commun 47:3544–3546
Rezaei Araghi R, Jäckel C, Cölfen H, Salwiczek M, Völkel A, Wagner SC, Wieczorek S, Baldauf C, Koksch B (2010) A β/γ motif to mimic α-helical turns in proteins. ChemBioChem 11:335–339
Robson Marsden H, Kros A (2010) Self-assembly of coiled coils in synthetic biology: inspiration and progress. Angew Chem Int Ed 49:2988–3005
Schuck P (2000) Size-distribution analysis of macromolecules by sedimentation velocity ultracentrifugation and Lamm equation modeling. Biophys J 78:1606–1619
Seebach D, Beck AK, Bierbaum DJ (2004) The world of β- and γ-peptides comprised of homologated proteinogenic amino acids and other components. Chem Biodivers 1:1111–1239
Vasudev PG, Ananda K, Chatterjee S, Aravinda S, Shamala N, Balaram P (2007) Hybrid Peptide Design. Hydrogen bonded conformations in peptides containing the stereochemically constrained β-amino acid residue, gabapentin. J Am Chem Soc 129:4039–4048
Woolfson DN (2005) The design of coiled-coil structures and assemblies. Adv Protein Chem 70:79–112
Yadav MK, Redman JE, Leman LJ, Alvarez-Gutiérrez JM, Zhang Y, Stout CD, Ghadiri MR (2005) Structure-based engineering of internal cavities in coiled-coil peptides. Biochemistry 44:9723–9732
Yoder NC, Kumar K (2006) Selective protein-protein interactions driven by a phenylalanine interface. J Am Chem Soc 128:188–191
Zhang Y, Kulp DW, Lear JD, DeGrado WF (2009) Experimental and computational evaluation of forces directing the association of transmembrane helices. J Am Chem Soc 131:11341–11343